J. Fluid Mech. (2014), *vol.* 739, *pp.* 229–253. © Cambridge University Press 2013
doi:10.1017/jfm.2013.612

The evolution of a stratified turbulent cloud

Andrea Maffioli[1],†, P. A. Davidson[1], S. B. Dalziel[2] and N. Swaminathan[1]

[1]Department of Engineering, University of Cambridge, Trumpington Street, Cambridge CB2 1PZ, UK

[2]Department of Applied Mathematics and Theoretical Physics, Centre for Mathematical Sciences, University of Cambridge, Wilberforce Road, Cambridge CB3 0WA, UK

(Received 21 December 2012; revised 19 June 2013; accepted 14 November 2013; first published online 17 December 2013)

Localized regions of turbulence, or turbulent clouds, in a stratified fluid are the subject of this study, which focuses on the edge dynamics occurring between the turbulence and the surrounding quiescent region. Through laboratory experiments and numerical simulations of stratified turbulent clouds, we confirm that the edge dynamics can be subdivided into materially driven intrusions and horizontally travelling internal wave-packets. Three-dimensional visualizations show that the internal gravity wave-packets are in fact large-scale pancake structures that grow out of the turbulent cloud into the adjacent quiescent region. The wave-packets were tracked in time, and it is found that their speed obeys the group speed relation for linear internal gravity waves. The energetics of the propagating waves, which include waveforms that are inclined with respect to the horizontal, are also considered and it is found that, after a period of two eddy turnover times, the internal gravity waves carry up to 16 % of the cloud kinetic energy into the initially quiescent region. Turbulent events in nature are often in the form of decaying turbulent clouds, and it is therefore suggested that internal gravity waves radiated from an initial cloud could play a significant role in the reorganization of energy and momentum in the atmosphere and oceans.

Key words: geophysical and geological flows, internal waves, stratified turbulence

1. Introduction

Turbulent flows in the presence of strong stable stratification occur in the atmosphere, oceans and lakes. Turbulence episodes in practice are often localized and without a continuous source of energy as a result of, for example, local shear instability or internal gravity wave breaking (see the review of Riley & Lelong 2000, and references therein). Localized regions of turbulence have been observed in the stratified oceanic thermocline by Grant, Moilliet & Vogel (1968), according to whom 'the most striking conclusions from this record are that there is turbulence in the thermocline and that it is in patches'. In the review of Gregg (1987) oceanic data are presented showing that mixing in the stratified ocean presents large-scale intermittency, which supports the idea of turbulence occurring in localized patches. Such patchiness of the turbulent activity on scales greater than the largest eddies has also been found by Mahrt (1989) when analysing atmospheric aircraft data. Motivated by these observations, we consider the problem of a localized and decaying region of

† Email address for correspondence: aplm2@cam.ac.uk

https://doi.org/10.1017/jfm.2013.612 Published online by Cambridge University Press

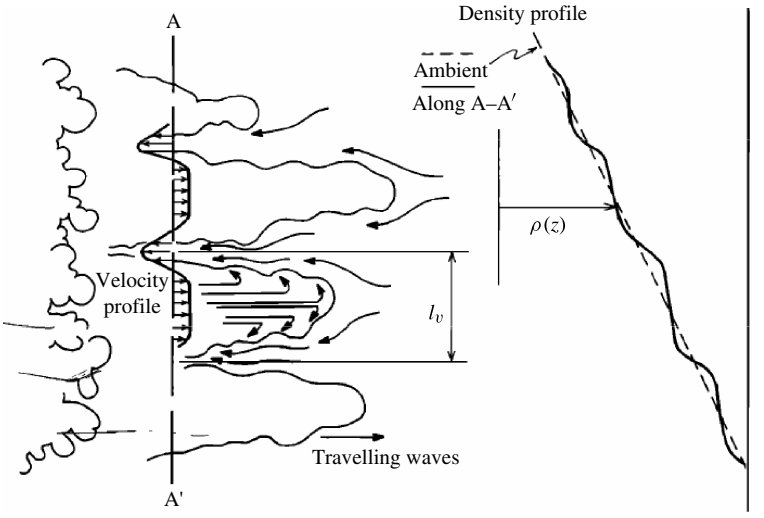


FIGURE 1. Sketch of motion of intrusions emerging from a stratified turbulent cloud. Return currents are established in between intrusions, with the resulting density profile across the intrusions given on the right of the image (reproduced from Browand, Guyomar & Yoon 1987 with permission).

turbulence sitting in an otherwise unperturbed and stably stratified environment. We call such a localized turbulent region a *turbulent cloud*; we consider stratified turbulent clouds, where the cloud interior and the surroundings are initially linearly stratified. Stratified turbulent clouds are governed by inhomogeneous dynamics, in contrast to the dynamics of homogeneous stratified turbulence. The latter class of problems has been covered extensively, with theoretical (see Billant & Chomaz 2001; Lindborg 2006), numerical (see Riley & de Bruyn Kops 2003; Waite & Bartello 2004; Brethouwer *et al.* 2007) and experimental approaches (see Fincham, Maxworthy & Spedding 1996; Praud, Fincham & Sommeria 2005). The inhomogeneous problem, on the other hand, has received relatively little attention, but its manifestation in nature makes it an interesting problem to study.

Turbulent clouds present a turbulent/non-turbulent interface between the cloud and its quiescent surroundings. A number of experimental studies on this interface and its dynamics were published some years ago (see Ivey & Corcos 1982; Thorpe 1982; Browand *et al.* 1987; De Silva & Fernando 1998). In all these experiments a grid is oscillated, either vertically or horizontally, in a stratified fluid creating a localized turbulent region, which after some time collapses under the effect of gravity with the formation of laterally spreading intrusions. Turbulent mixing in the intrusion interiors results in smaller absolute density gradients compared to the ambient linear stratification; these horizontal density differences lead to horizontal pressure gradients that push the intrusions forwards into the quiescent region (see figure 1). The displacement of dye lines in the initially quiescent region is a signature of internal wave emission from the turbulent cloud, which was observed by some authors (see Browand *et al.* 1987; De Silva & Fernando 1998). Browand *et al.* (1987) interpret the waves as being horizontally travelling columnar modes excited by the motion of the intrusions. Columnar modes are known to propagate in front of single intrusive gravity currents generated by the release of mixed fluid of intermediate density in a

https://doi.org/10.1017/jfm.2013.612 Published online by Cambridge University Press

stratified container (see Manins 1976). Density-driven intrusions with their associated staircase-like density profiles have been observed in lakes (see e.g. Caldwell, Brubaker & Neal 1978; Hogg *et al.* 2013) and in the ocean (see Armi 1978).

In a recent numerical study, Basak & Sarkar (2006) considered the evolution of a horizontal shear layer in a fluid with a vertical stable density gradient. The horizontal shear layer, initialized with broadband fluctuations, rapidly undergoes transition to turbulence with the formation of a turbulent cloud surrounded by two opposite-moving laminar streams. The edge dynamics are considered and intrusions spreading into the surrounding streams are observed. The internal wave field is highlighted using the horizontal divergence $-\partial u_z/\partial z$ (u_z is the vertical component of velocity), although this tool cannot identify any horizontal waves which are present in the problem (horizontal wave modes, as we will see, do not possess any vertical velocity). When using horizontal divergence as a signature of internal wave emission, inclined wave beams are found to propagate in the quiescent region.

Turbulent wakes are another example of a localized turbulent region and several laboratory experiments and numerical simulations have treated the dynamics of stratified turbulent wakes including the radiated internal wave field (Gilreath & Brandt 1985; Bonneton, Chomaz & Hopfinger 1993; Lin, Boyer & Fernando 1993; Spedding, Browand & Fincham 1996; Diamessis, Domaradzki & Hesthaven 2005; Abdilghanie & Diamessis 2013). Stationary lee waves generated by a sphere or body moving with respect to the stratified fluid are observed, in addition to 'random internal waves' (Gilreath & Brandt 1985) that are observed to propagate with an inclination angle with respect to the horizontal plane (Bonneton *et al.* 1993; Diamessis *et al.* 2005; Abdilghanie & Diamessis 2013). Gravitational collapse of the wake could give rise to intrusions growing in the spanwise direction and forcing horizontal internal gravity waves. However, due to the little mixing occurring within the wake, clear intrusions have not been clearly observed in stratified wake experiments and simulations, which lead some authors to discount this mechanism as a significant source of internal gravity wave generation (see Lin *et al.* 1993) and even to put into question the fact that high-Froude-number stratified turbulent wakes eventually collapse under gravity (see Abdilghanie & Diamessis 2013). The absence of layered intrusions in stratified wakes makes the problem quite distinct from the turbulent cloud problem under consideration, where intrusions are known to exist and are a prominent feature of the edge dynamics.

In the context of homogeneous stratified turbulence, it has been known for a long time (see Lin & Pao 1979; Kimura & Herring 1996) that initially isotropic turbulence in a stratified fluid rapidly becomes anisotropic, with the formation of pancake-like structures in its interior. The formation of the pancakes is sometimes known as layering and its causes are as yet unclear, with a number of mechanisms having been put forward over the years, for example the decorrelation instability of Lilly (1983) and the zig-zag instability (see Billant & Chomaz 2000). It should be noted that both the zig-zag and decorrelation instability mainly affect the potential vorticity component of the flow (or vortical mode, see Riley & Lelong 2000); no layering mechanisms involving the internal wave component have been proposed thus far. In the case of the zig-zag instability acting on a columnar vortex pair, it is not clear how this layering mechanism would manifest itself in turbulence that is initially isotropic.

There are a number of analogies between stratified and rotating turbulent flows: both classes of turbulence display anisotropic structures in their interior (the structures are elongated along the rotation axis in rotating turbulence), and both stratified and rotating fluids sustain wave propagation in their interior. In a rotating fluid the restoring force is provided by the Coriolis force, which is responsible for oscillations in the interior of the fluid known as inertial waves (Lighthill 1978). Recently,

https://doi.org/10.1017/jfm.2013.612 Published online by Cambridge University Press

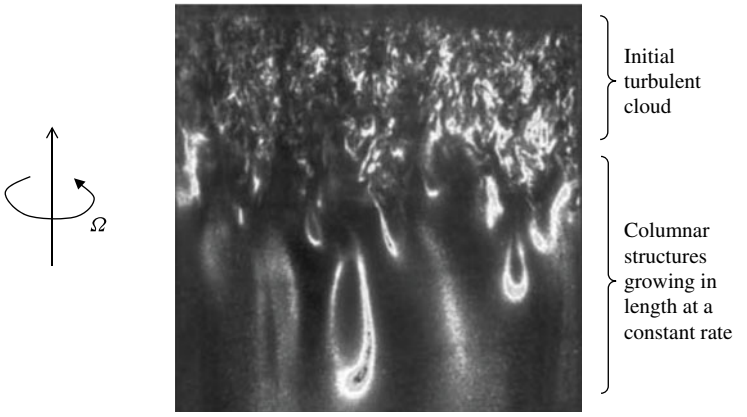


FIGURE 2. Image of the flow in rotating turbulent cloud experiment by Davidson *et al.* (2006). The turbulent cloud was initially confined to the top of the image; image taken at a time $\Omega t = 10$ after initiation of the turbulence (Ω is the system rotation rate about the vertical axis).

Davidson, Staplehurst & Dalziel (2006) proposed a theory according to which an isolated eddy in a rotating environment deforms into a columnar structure as a result of linear inertial wave propagation. This result could also be relevant for turbulent clouds composed of a multitude of eddies. The authors also present the results from experiments on a turbulent cloud in a rotating system showing that columnar structures emerge from the cloud and grow into the quiescent region (see figure 2). The structures are indeed found to be created by the linear superposition of inertial waves, as demonstrated by comparing their growth rate to the linear group speed of inertial waves. These results provide motivation for studying similar internal gravity wave mechanisms in the context of stratified turbulent clouds.

Having considered the previous work on turbulent clouds in stratified fluids, we have identified a number of open questions regarding this flow. First, is there a manifestation of pancake formation or layering in this inhomogeneous problem? If so, what causes the formation of pancakes in the flow? Additionally, what is the complete internal wave dispersion pattern from the turbulent cloud? Finally, are the internal waves linear and how much energy do they carry away from the cloud? We attempt to answer these questions using laboratory experiments and numerical simulations in conjunction.

The remainder of this paper is structured as follows: in § 2 results from laboratory experiments on stratified turbulent clouds are presented, and in § 3 direct numerical simulations of the problem are described and discussed. A discussion follows in § 4 comparing and contrasting the experiments and the DNS, and exploring in more detail the analogy between stratified and rotating turbulent clouds. Finally a brief set of concluding remarks is given in § 5. Throughout the paper we sometimes use the following abbreviations: DNS for direct numerical simulation, IGW for internal gravity wave and PV for potential vorticity.

2. An experiment on turbulent clouds in a stratified fluid

We have performed a variant of the experiments of Thorpe (1982) and Browand *et al.* (1987). Browand *et al.* (1987) created a cloud of turbulence in a stratified

https://doi.org/10.1017/jfm.2013.612 Published online by Cambridge University Press

fluid by continuously oscillating a grid. The turbulence initially occupies only a small part of the tank, but then spreads in the horizontal direction, with the formation of horizontal intrusions as evidenced by dye initially inserted in the turbulent cloud. We have repeated their experiment except that, instead of continuously oscillating the grid, we oscillate it just once in the horizontal direction and restrict this motion to the right-half of the tank, creating an initial cloud of turbulence which is then free to evolve (this is similar to the experiments of Liu, Maxworthy & Spedding 1987). The tank we used is 105 cm long, 26 cm wide and 52 cm deep, filled with a linearly stratified salt solution to a depth of 45 cm. The linear stratification was established using the standard double-bucket method (Fortuin 1960). To create turbulence in the tank we used a rake of vertical bars so as to avoid any externally imposed vertical length scale (the vertical scale is instead selected by the dynamics); the rake is composed of vertical bars with a bar size $b = 6.4$ mm and bar spacing $M = 31.8$ mm. The amplitude of the initial oscillation was $\sim$40 cm, which defines the initial horizontal extent of the turbulent cloud, and three rake speeds were utilized: $U \approx 8, 14, 28$ cm s^{-1}. The rake was set into motion from the right-end of the tank, it was then traversed at a uniform speed up to the centre of the tank, and then traversed uniformly back to its original position. Decaying turbulence experiments in a non-stratified fluid were performed with grids of the same bar and mesh size driven at similar speeds U by Dalziel (1992) and Staplehurst (2007) and they found that, at the beginning of the power-law region $u^2 \sim t^{-n}$, typical velocities and length scales of the turbulence are $u \approx 0.05U$ and $l \approx b$. We take these as estimates of u and l at the beginning of the decay in our stratified experiments also, since the initial Froude number is $Fr_0 \gtrsim 1$ in all runs. Experiments were carried out with different initial linear stratifications, with Brunt–Väisälä frequencies $N = \sqrt{(g/\rho_0)\,|\mathrm{d}\rho/\mathrm{d}z|}$ (ρ_0 is a reference density taken as the density of the water close to the free surface) in the range $N = 0.6$–1.4 rad s^{-1}. The initial Froude number based on turbulence quantities, $Fr_0 = u/Nl$, lies in the range $Fr_0 = 0.8$–3.6.

The turbulence was visualized using two techniques: in some experiments pearlessence flakes, which highlight regions of strong shear (Savaş 1985), were distributed throughout the salt solution (this was achieved by adding the pearlessence to the double-bucket system before filling the tank), while in others fluorescein (a green fluorescent dye) was added to the initial turbulent cloud. The flow was illuminated with a vertical light sheet and images of reflected light intensity captured by a digital camera, viewing in the plane shown in the schematic of figure 3.

Dye marks fluid motion and hence our fluorescein experiments highlight the deformation of the cloud edge due to the turbulent advection of fluid. In contrast, pearlessence is distributed throughout the tank, and therefore shows both the turbulent motion of the fluid initially in the cloud and any internal waves propagating in the quiescent region adjacent to the cloud. Pairs of nominally identical experiments were carried out, using in one case pearlessence flakes and in the other case fluorescein. This results in two sets of images for the same experimental conditions, which can be compared and contrasted. In particular, by 'subtracting off' the dyed region shown by the fluorescein images from the pearlessence images, a signature of the wave dispersion from the turbulent cloud is obtained.

Figure 4 shows fluorescein and pearlessence images obtained under the same experimental conditions. In both sets of images horizontal layered structures are seen to emerge from the edge of the turbulent cloud and grow into the quiescent region. From the time of the second frame shown onwards, the horizontal extent of the structures is different across the two visualizations, with the pearlessence structures

https://doi.org/10.1017/jfm.2013.612 Published online by Cambridge University Press

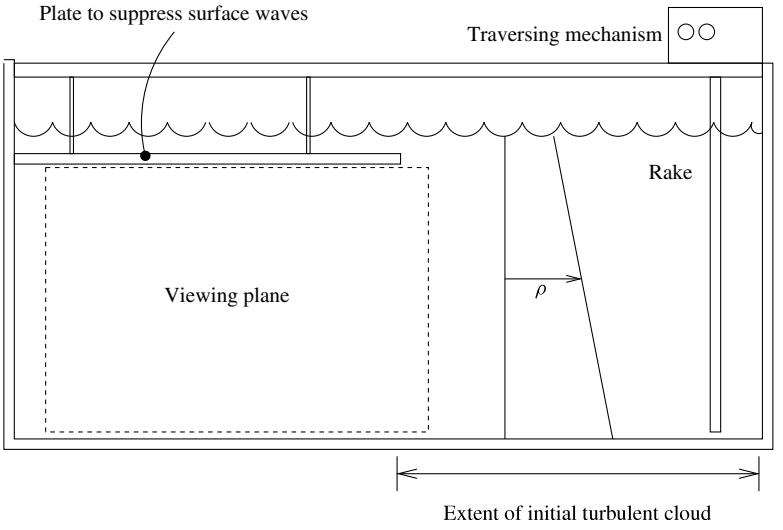


FIGURE 3. Experimental set-up.

extending far beyond the fluorescein structures. It would therefore appear that the two types of structures visualized are not the same physical structure. By considering in the pearlessence images only the structures that have extended beyond the dyed region of fluid, we can say that these elongated horizontal structures must be associated with the internal wave field. We are therefore in the presence of layered structures created by the superposition of internal gravity waves. The vertical length scale associated with the pearlessence and the fluorescein structures is roughly the same, and hence it is likely that, as suggested by Browand *et al.* (1987), the intrusions marked by the dye excite horizontally travelling waves. The presence of horizontal fluid intrusions as well as horizontally travelling internal waves in the stratified turbulent cloud problem is different to what happens in the rotating cloud problem, where only vertically travelling waves are seen to emerge from the turbulent cloud (Davidson *et al.* 2006). We will return to this point in the discussion section.

In summary, we have performed experiments with stratified turbulent clouds that show the appearance of horizontally elongated wave-packets propagating ahead of horizontal fluid intrusions. The tools we have used are essentially qualitative, consisting of different flow visualization techniques. The physical picture obtained from these simple experiments motivated us to study the turbulent cloud problem further using quantitative tools. Our approach has been to use direct numerical simulations to study the wave dispersion from the cloud more in detail, particularly to check the possible linearity of the waves and consider their energetics. The results we obtained are presented below.

3. Direct numerical simulations

3.1. *Numerical methods*

Motivated by our experimental inspection of stratified turbulent clouds, we performed numerical simulations of a localized region of turbulence in a stratified fluid. The numerical methodology we employed consists of solving the Boussinesq set of

https://doi.org/10.1017/jfm.2013.612 Published online by Cambridge University Press

https://doi.org/10.1017/jfm.2013.612 Published online by Cambridge University Press

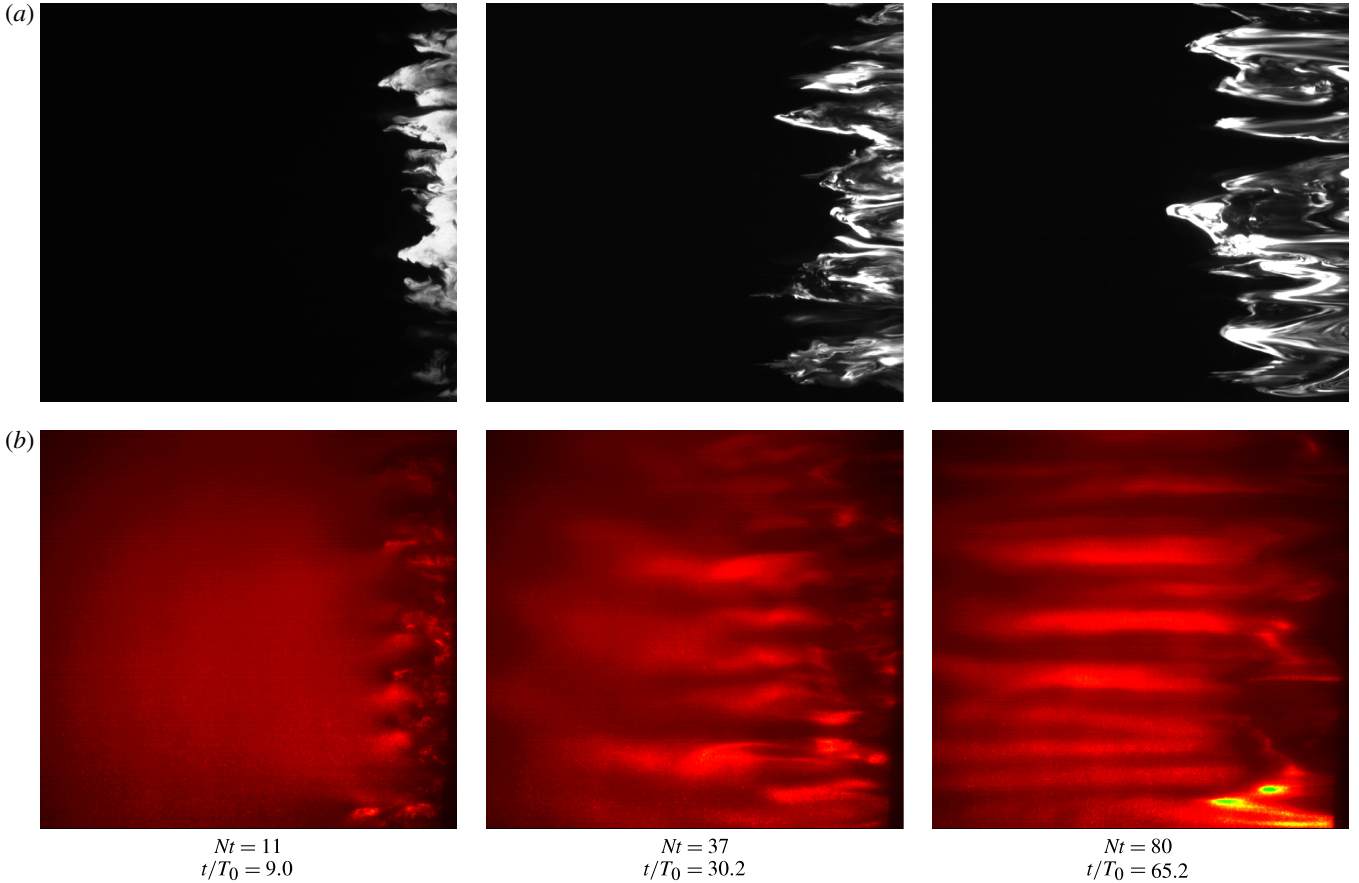


FIGURE 4. (Colour online) Flow visualization of the edge of a stratified turbulent cloud at three different times: (*a*) fluorescein visualization, (*b*) pearlessence visualization. Experimental parameters: $U = 14.5$ cm s^{-1}, $N = 1.4$ rad s^{-1}. The initial integral time scale T_0 is estimated as $T_0 = l/u = 0.88$ s with $u = 0.73$ cm s^{-1} and $l = 0.64$ cm.

equations directly for a linearly stratified fluid. This set of equations can be written as:

$$\nabla \cdot \boldsymbol{u} = 0, \tag{3.1}$$

$$\frac{\partial \boldsymbol{u}}{\partial t} + \boldsymbol{u} \cdot \nabla \boldsymbol{u} = -\frac{1}{\rho_0}\nabla p + b\,\boldsymbol{e}_z + \nu \nabla^2 \boldsymbol{u}, \tag{3.2}$$

$$\frac{\partial b}{\partial t} + \boldsymbol{u} \cdot \nabla b = -N^2 u_z + \mathscr{D}\nabla^2 b, \tag{3.3}$$

where $\boldsymbol{u}$ is the velocity vector, u_z the vertical component of velocity, p the perturbation pressure from the hydrostatic pressure distribution, ν the kinematic viscosity, $\mathscr{D}$ the density diffusivity and b the buoyancy defined as $b = -g\rho'/\rho_0$ (where ρ' is the perturbation density from the linear density profile and gravity is acting in the vertical z direction). The Brunt–Väisälä frequency N is taken as a constant input parameter in the simulations. Equation (3.3) for the buoyancy is obtained either from the energy equation, if the stratification is due to temperature differences, or from the equation for the concentration of a constituent (e.g. salt in water), if the stratification is due to variations of constituent concentration in the fluid (Kundu & Cohen 2004). Equations (3.1)–(3.3) are solved using a pseudo-spectral method based on Rogallo's algorithm (see Yeung 2001). The numerical domain is a cube of size l_{box}, and the boundary conditions are periodic in all three directions. Time advancement is carried out using a second-order Runge–Kutta predictor–corrector integration scheme, while the viscous and diffusive terms are integrated exactly by using suitable integrating factors. De-aliasing of the nonlinear terms is performed using a combination of truncation and phase-shifting.

The decaying stratified simulations were initialized with a fully developed field of turbulence obtained from a homogeneous isotropic pre-computation in a constant-density fluid. The pre-computation was initialized with random Fourier modes satisfying a prescribed energy spectrum of the form $E(k) = Ak^4 \exp(-k^2/a^2)$, where A and a are input parameters. During the pre-computation this artificial velocity field is allowed to evolve until the velocity derivative skewness S reaches an approximately steady value at $S \approx -0.5$ (Davidson 2004). If k_{max} is the maximum resolved wavenumber, and η and l the Kolmogorov and integral length scales at the end of the pre-computation, we only retained the pre-computations with $k_{max}\eta \geqslant 1.5$ and $l_{box}/l > 10$. This ensures that the small scales are resolved and that the large scales are not too 'boxed-in' (see Pope 2000). The fully developed turbulence thus obtained is then confined to a central slice of the cube by applying a high-order exponential filter, which suppresses velocity fluctuations outside the central region. The width of the filter is $0.2l_{box}$. We use this localized turbulent field, an example of which is given in figure 5, to initialize the stratified simulations. The buoyancy field is initialized with $b = 0$ everywhere in the domain so that at the beginning of the stratified simulations the density profile is linear throughout the periodic cube, i.e. no mixing has initially taken place within the cloud.

In a single run, Lagrangian particles were added to the simulation. Lagrangian particles consist of idealized fluid elements whose position can be found by integrating $\mathrm{d}\boldsymbol{r}/\mathrm{d}t = \boldsymbol{u}(t, \boldsymbol{r})$, where $\boldsymbol{u}$ is the fluid velocity at $\boldsymbol{r}$. A second-order predictor–corrector scheme is used to find the position of the particles. Since the Eulerian velocity field is only available at the discrete grid nodes, interpolation has to be used to find the fluid velocity at the particle positions. This interpolation is the dominant source of error in the extraction of Lagrangian data (Yeung & Pope 1989); in the numerical code

https://doi.org/10.1017/jfm.2013.612 Published online by Cambridge University Press

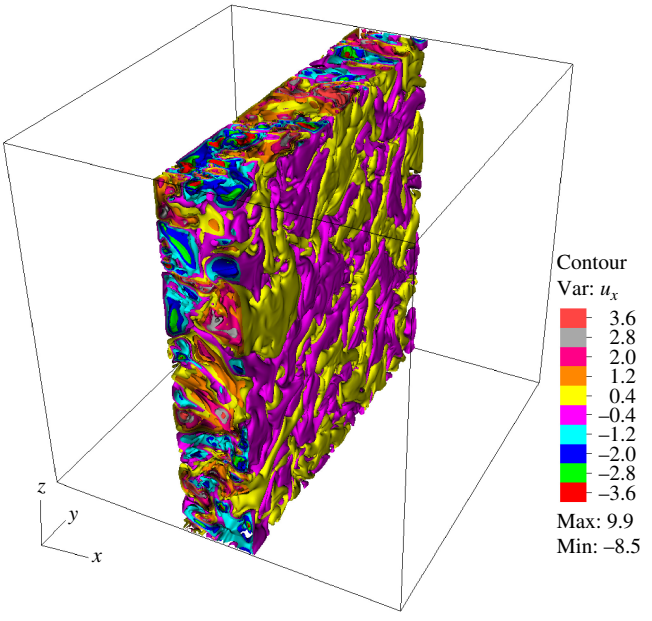


FIGURE 5. (Colour online) Initial condition for stratified DNS: iso-surfaces of u_x from fully developed turbulence confined to a vertical slice.

fourth-order cubic splines are used to accurately interpolate Eulerian velocity field data.

3.2. *Eulerian visualizations*

We now present numerical simulation results, starting from Eulerian visualizations of the flow field. The simulations we performed are listed in table 1, together with the relevant initial parameters and durations of the decaying turbulence simulations. The simulations are named based on their initial Froude number, for example case F0.1 corresponds to a simulation with $Fr_0 = 0.1$. In listing the initial quantities of the different simulations we do not distinguish between horizontal and vertical directions, as one normally would do in stratified turbulence simulations. The reason behind this is that the initial conditions for all stratified runs are isotropic within the cloud, coming from a pre-computation in a constant-density fluid. For all cases the Schmidt number is taken as $Sc = 1$.

Figure 6 shows iso-surfaces of u_x, the velocity component in the x-direction, for case F0.1 at different times throughout the simulation. The structure of the u_x field rapidly becomes pancake-like, with the growth of horizontal flattened structures out of the turbulent cloud and into the quiescent region. In some cases the pancakes detach from the cloud forming isolated structures. The pancakes maintain their coherence for a time interval Δt in the range $N\Delta t = 5$–10, after which they either reach the cube boundaries or their corresponding iso-surface appears to slowly disappear. As the isovalues are kept constant across successive snapshots, the latter case could be due to a reduction in energy density as the kinetic energy spreads out of the initial turbulent cloud or to the gradual action of viscous dissipation. By $Nt = 19.8$ most of the structures have reached the cube boundaries and start to influence the structures on the opposite edge because of periodicity.

https://doi.org/10.1017/jfm.2013.612 Published online by Cambridge University Press

Run	Resol.	Fr_0	Re_0	$\mathscr{R}_0$	N (rad s^{-1})	l_{box}/l_0	$k_{max}\eta_0$	t_{end}/T_0	Nt_{end}
F0.03	512^3	0.032	485	0.5	44.5	10.7	1.6	1.3	41.8
F0.1	512^3	0.1	371	3.7	44.5	15.4	1.5	2.7	27.1
F0.2	512^3	0.2	371	14.8	22.2	15.4	1.5	3.0	15.5
F0.2ext	512^3	0.2	371	14.8	22.2	15.4	1.5	18.5	410.7
F1.5	512^3	1.5	371	—	3.0	15.4	1.5	22.5	15.5

TABLE 1. Simulation parameters for the different runs considered. In all cases the subscript 0 on a certain quantity corresponds to the initial value of the quantity at $t = 0$. The quantity T_0 corresponds to the initial integral time scale $T_0 = l_0/u_0$. The Reynolds number is $Re_0 = u_0 l_0/\nu$. The buoyancy Reynolds number is given at the start of each run as $\mathscr{R}_0 = Re_0 Fr_0^2$ since the turbulence is initially isotropic (we do not give this quantity for the case F1.5 since the Froude number is initially high, far away from being a strongly stratified case). The Kolmogorov scale at the start of the stratified runs is $\eta_0 = (\nu^3/\epsilon_0)^{1/4}$, where ϵ is the kinetic energy dissipation rate.

In figure 7 iso-surfaces are shown for a number of quantities at a late time. Figure 7(*a*) is a snapshot of the potential vorticity field Π, which is computed as $\Pi = \boldsymbol{\zeta} \cdot \nabla \tilde{b} = N^2 \zeta_z + \boldsymbol{\zeta} \cdot \nabla b$ ($\boldsymbol{\zeta} = \nabla \times \boldsymbol{u}$ is the vorticity and $\tilde{b}$ is the 'total buoyancy', $\tilde{b} = N^2 z + b$). This quantity has the property of being materially conserved in a stratified flow, apart from viscous and diffusive effects (Riley & Lelong 2000). We therefore use Π as tracer to emphasize turbulent advection from and within the cloud, similarly to the dye used in our experiments. The other iso-surfaces given in figure 7 are for u_x, u_y and b; these quantities are not materially conserved and their fields will be re-arranged both by turbulent advection and by any internal waves present in the simulation. The Π field remains compact at the late time and its extent does not differ greatly from the initial extent of the turbulent cloud. On the other hand, the other three fields present large-scale pancakes extending up to the edge of the domain. Using similar reasoning as in § 2, it can be concluded that the large-scale pancakes highlighted by the plots in figures 6 and 7 are internal waves propagating in the quiescent region. These pancake structures are nothing but the three-dimensional equivalent of the horizontal structures evidenced in the experiments with pearlessence (see figure 4).

As pointed out by Riley & Lelong (2000), there could be motions in a stratified flow that do not possess potential vorticity but which are not internal waves. It is possible that such advective motions could be causing the large-scale structures observed in our runs, which would invalidate our interpretation of them being the result of the superposition of internal waves. To dispel any doubts regarding the nature of the pancakes, we seeded the initial turbulent cloud with Lagrangian particles. This was done for a single case, run F0.1, and the results are presented in the next section.

3.3. *Lagrangian visualizations*

Inertia-less particles were randomly distributed throughout the initial turbulent cloud for case F0.1. The displacement of the particles at a certain time can be compared with the extent of the pancake structures from figures 6 and 7. If the particles are displaced up to the edge of the pancakes then it is likely that these structures are caused by advection of fluid from the cloud. By contrast, if the pancakes lie ahead of the particles, internal waves are probably at the origin of these large-scale motions (as the motions are beyond the region of action of turbulent advection).

https://doi.org/10.1017/jfm.2013.612 Published online by Cambridge University Press

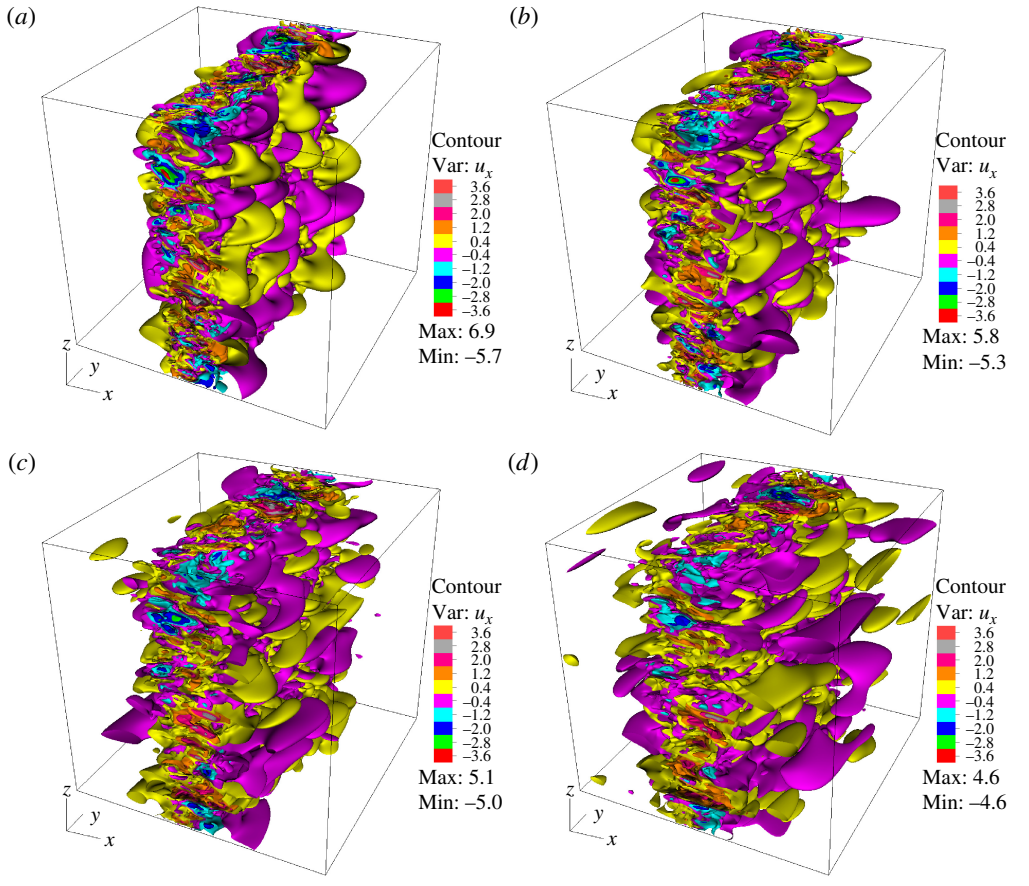


FIGURE 6. (Colour online) Iso-surfaces of constant u_x with each colour corresponding to a different isovalue. Case F0.1 at four different times: (*a*) $Nt = 4.7$, (*b*) $Nt = 8.3$, (*c*) $Nt = 13.5$, (*d*) $Nt = 19.8$.

The particle positions at two times are shown in figure 8. The two lowest iso-surfaces of u_x showing the pancake structures have been superimposed on the particle positions for visual aid. It is clear from the figure that at the early time of $Nt = 9.6$ the particles are confined to a region close to the initial turbulent cloud, whereas the u_x field propagates ahead in the quiescent region. This is even more evident at the later time $Nt = 19.6$. These results confirm that the pancake motions in this inhomogeneous problem are created by the superposition of internal waves.

To justify our use of potential vorticity as a tracer in § 3.2 we plot the particle positions superimposed on two iso-surfaces of Π at a late time in figure 9. The Eulerian and Lagrangian fields match closely, but there are some discrepancies at the edge of the cloud which could be due to the choice of the iso-surface levels. This result suggests that fluid advection that does not contain potential vorticity is negligible in our simulations.

3.4. *Are the pancakes composed of linear waves?*

Having confirmed that large-scale pancake structures are created in the turbulent cloud problem by the superposition of internal waves, a natural question that arises is: are

https://doi.org/10.1017/jfm.2013.612 Published online by Cambridge University Press

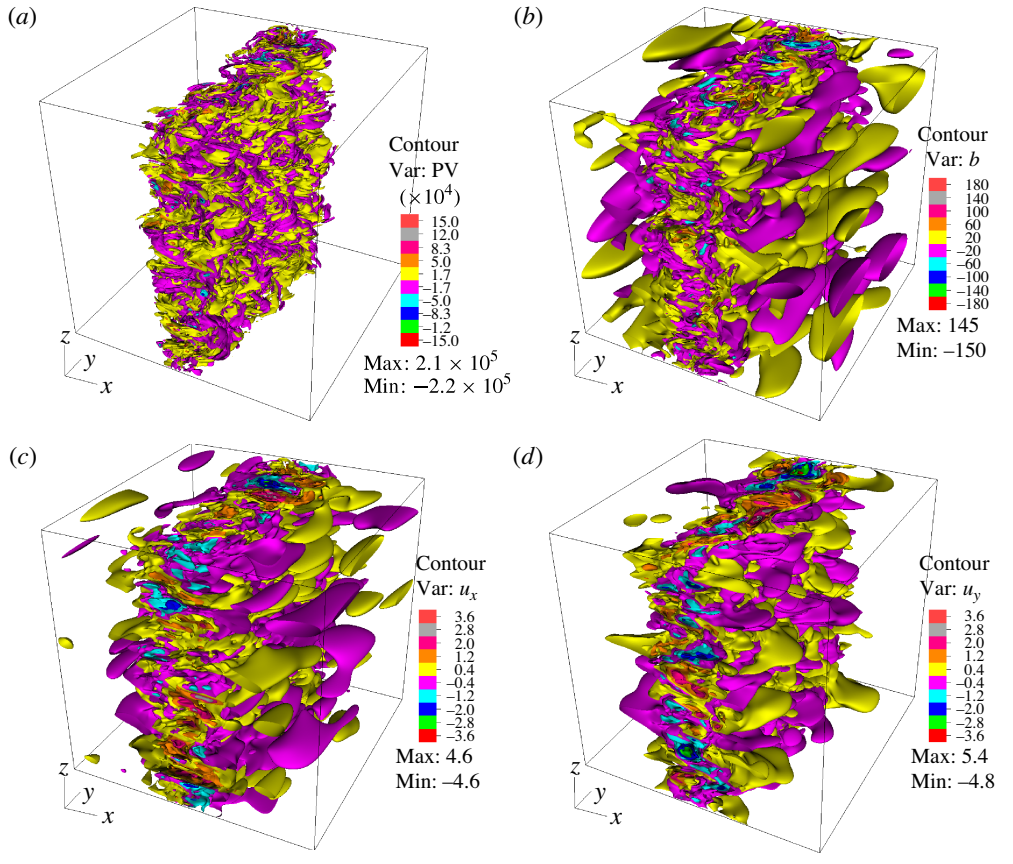


FIGURE 7. (Colour online) Iso-surfaces at time $Nt = 19.8$ for case F0.1: (*a*) potential vorticity Π, (*b*) buoyancy b, (*c*) u_x, (*d*) u_y.

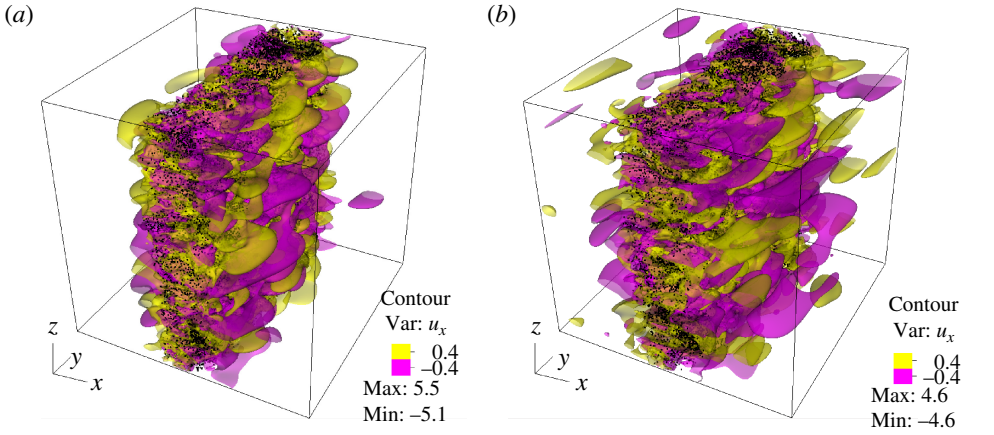


FIGURE 8. (Colour online) Particle positions superimposed on the two lowest iso-surfaces of u_x for case F0.1 at two times: (*a*) $Nt = 9.6$, (*b*) $Nt = 19.8$. Each black dot corresponds to a Lagrangian particle.

https://doi.org/10.1017/jfm.2013.612 Published online by Cambridge University Press

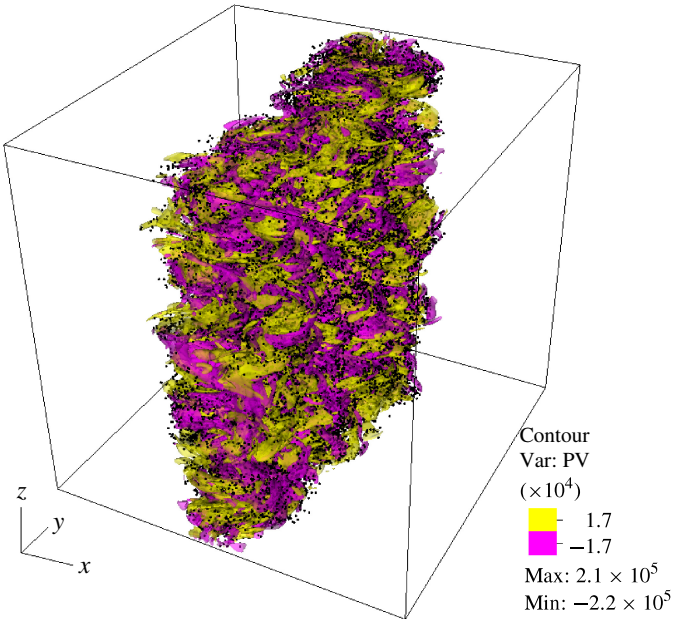


FIGURE 9. (Colour online) Particle positions superimposed on the two lowest iso-surfaces of Π from figure 7. Case F0.1 at time $Nt = 19.8$.

these waves linear or nonlinear? Because the structures created by the waves can be thought of as wave-packets travelling at the group speed, another way of posing this question would be: do the pancake-shaped wave-packets travel at the group speed as predicted by linear theory?

To answer this question our approach is to track individual pancakes from u_x iso-surface plots and compare their speed with the expected linear group speed. As can be appreciated by inspection of figure 6, the pancake structures elongate primarily in the x-direction because the forcing of the intrusions is predominantly in the direction of the inhomogeneity, i.e. the x-direction. Therefore the tracking works by focusing in on an individual pancake-shaped wave-packet – corresponding to an iso-surface with a specific isovalue – and finding the maximum extension along the x-axis of its iso-surface. The maximum x-extension of the wave-packet corresponds to the wave-packet front. This procedure is repeated for successive time steps, and hence plots of wave-packet front displacement against time can be computed. Such plots are presented in figure 10 for a collection of pancake-shaped wave-packets taken from the low-Froude-number simulations, runs F0.03, F0.1 and F0.2. The wave-packet displacement grows linearly with time, meaning that the group speed (given by the slope of the curves) is constant, a result which is consistent with linear wave propagation.

The expression for the group velocity of internal gravity waves can be written as (see Kundu & Cohen 2004)

$$\boldsymbol{c}_g = \pm \frac{N k_z}{k^3} (k_z \boldsymbol{e}_h - k_h \boldsymbol{e}_z), \tag{3.4}$$

where k_z and k_h are the vertical and horizontal wavenumbers so that the wavevector $\boldsymbol{k}$ is given by $\boldsymbol{k} = k_h \boldsymbol{e}_h + k_z \boldsymbol{e}_z$, and $k = |\boldsymbol{k}|$. We are in the presence of horizontally travelling wave-packets meaning that the wavevector must be purely vertical

https://doi.org/10.1017/jfm.2013.612 Published online by Cambridge University Press

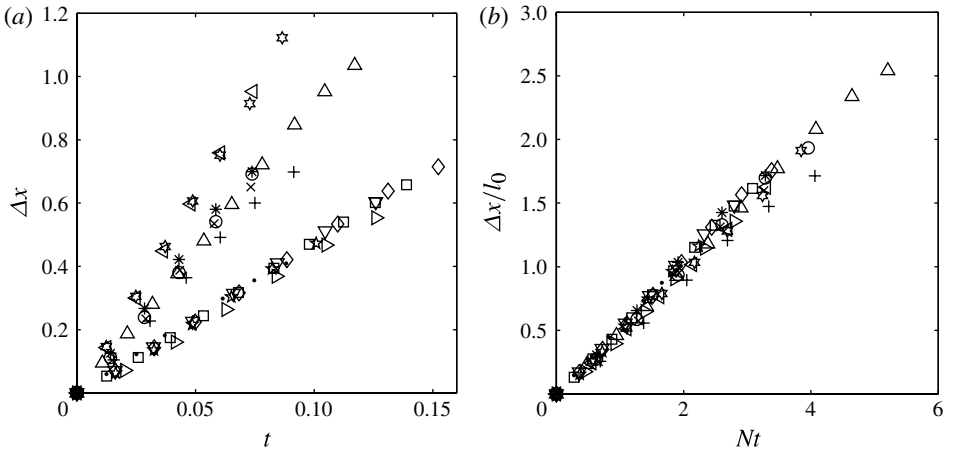


FIGURE 10. Displacement of the front of 13 different wave-packets tracked in simulations F0.03, F0.1, F0.2 as a function of time. Different symbols correspond to different individual wave-packets. In (*b*) Δx and t are normalized by the initial integral length scale l_0 and N^{-1} respectively.

with $k_h = 0$. An expression for the group velocity according to linear theory is therefore $\boldsymbol{c}_g = \pm(N/k_z)\boldsymbol{e}_h = \pm(N\lambda_z/2\pi)\boldsymbol{e}_h$, where λ_z is the vertical wavelength. We therefore would expect the horizontal internal waves created by the initially isotropic turbulent cloud to have a group speed $c_g \sim Nl_0$, if linear theory applies. To check if the wave-packets are indeed composed of linear internal gravity waves, figure 10(*b*) shows the same data as in figure 10(*a*) but with displacement normalized by the initial integral length scale l_0 and time non-dimensionalized by multiplication by N. If the horizontally travelling waves are linear the curves should collapse on a single straight line and indeed they do.

So far we have verified the proportionality of the group speed c_g to N and l_0, but we have not confirmed the value of the constant that ensures the exact expression $c_g = N/k_z$ is enforced. To check that $c_g = N/k_z$ in the simulations, we considered vertical slices at an x location in the initially quiescent region, with snapshots taken after the passage of the wave-packets. There is a clear vertical wavelength associated with the u_x field in such vertical slices (see figure 11) and we extracted the dominant vertical wavenumber k_z by taking the two-dimensional fast Fourier transform of these fields. It was hence possible to calculate $c_g = N/k_z$ and compare it with the group speed obtained from the wave-packet tracking. The results are presented in table 2; more than one wave-packet was tracked for every run so an average wave-packet group speed was calculated for every simulation. For all three low-Fr runs the wave-packet c_g compares well with the expected group speed from linear theory.

In summary, then, we have tested the linearity of the internal waves composing the pancake structures, and the results show that the waves do indeed act as linear internal gravity waves. However, as can be appreciated from figure 6, the horizontal internal waves are of finite amplitude and we therefore refer to them as *quasi-linear waves*.

3.5. *Wave dispersion pattern*

It is of interest to study the internal wave dispersion pattern from the turbulent cloud. We have already confirmed the presence of horizontally travelling waves (with frequency $\omega \approx 0$) in the simulation, but we expect a spectrum of frequencies in the radiated wave field since the initial turbulent cloud contains wavevectors $\boldsymbol{k}$

https://doi.org/10.1017/jfm.2013.612 Published online by Cambridge University Press

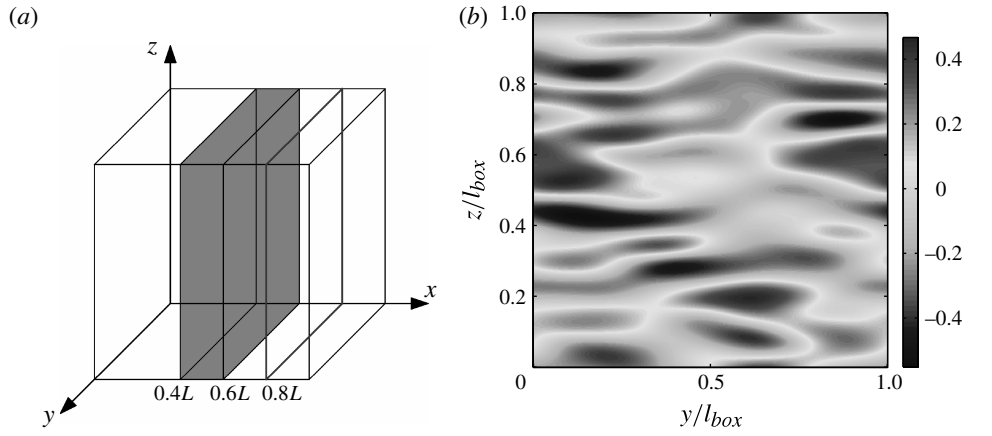


FIGURE 11. Vertical slice in the quiescent region after wave passage. In (*a*) the black line at $0.8\,L$ shows the location of the slice, while the grey area corresponds to the initial extent of the turbulent cloud. The snapshot in (*b*) was taken at a time $Nt = 13.5$ and the shading shows the u_x field on the slice.

Run	N	k_z at $\lvert\hat{u}_x^{2D}\rvert_{max}$	$c_g = N/k_z$	Wave-packet c_g
F0.03	44.5	3.5	12.7	12.9
F0.1	44.5	5	8.9	9.1
F0.2	22.2	4.5	4.9	4.8

TABLE 2. Comparison of group speed as expected from linear theory with measured wave-packet speed. The wave-packet c_g was averaged over all wave-packets tracked from an individual run. Only low-*Fr* runs are considered.

in all directions. Internal gravity waves with frequencies in the range $0 \leqslant \omega \leqslant N$ are expected according to the linear dispersion relation $\omega = Nk_h/k$. To highlight off-axis waves we use $\partial u_z/\partial z$, the negative horizontal divergence, which has been used previously by a number of authors as a signature of the wave field emitted by a turbulent cloud (Spedding *et al.* 1996; Diamessis *et al.* 2005; Basak & Sarkar 2006). It should be emphasized, however, that the $\partial u_z/\partial z$ field cannot show horizontal internal waves with $\boldsymbol{k} = k_z\boldsymbol{e}_z$ that contain purely horizontal velocity (by continuity $\boldsymbol{k}\cdot\boldsymbol{u} = 0$ for linear internal gravity waves), and hence the u_x field is used to show these zero-frequency waves.

Figure 12 contains x–z slices of the u_x and $\partial u_z/\partial z$ fields at two times for run F0.1. As previously seen in the three-dimensional visualizations of § 3.2, the u_x field shows the presence of horizontal internal waves in the initially quiescent region. The horizontal waves are clearly visible from the time $Nt = 10.9$ and create a close-to-uniform layering, similarly to the experimental slices of figure 4. At this early time, diagonal waves highlighted by $\partial u_z/\partial z$ have not propagated far from the initial turbulent region, which could be because, from (3.4), their horizontal group speed $c_{gh} = Nk_z^2/k^3 = (N/k_z)\sin^3\Theta$ is lower than the (horizontal) group speed of purely horizontally propagating waves $c_g = N/k_z$. By the later time $Nt = 32.2$ both waveforms (horizontal and diagonal) have filled the computational domain. The typical angle of

https://doi.org/10.1017/jfm.2013.612 Published online by Cambridge University Press

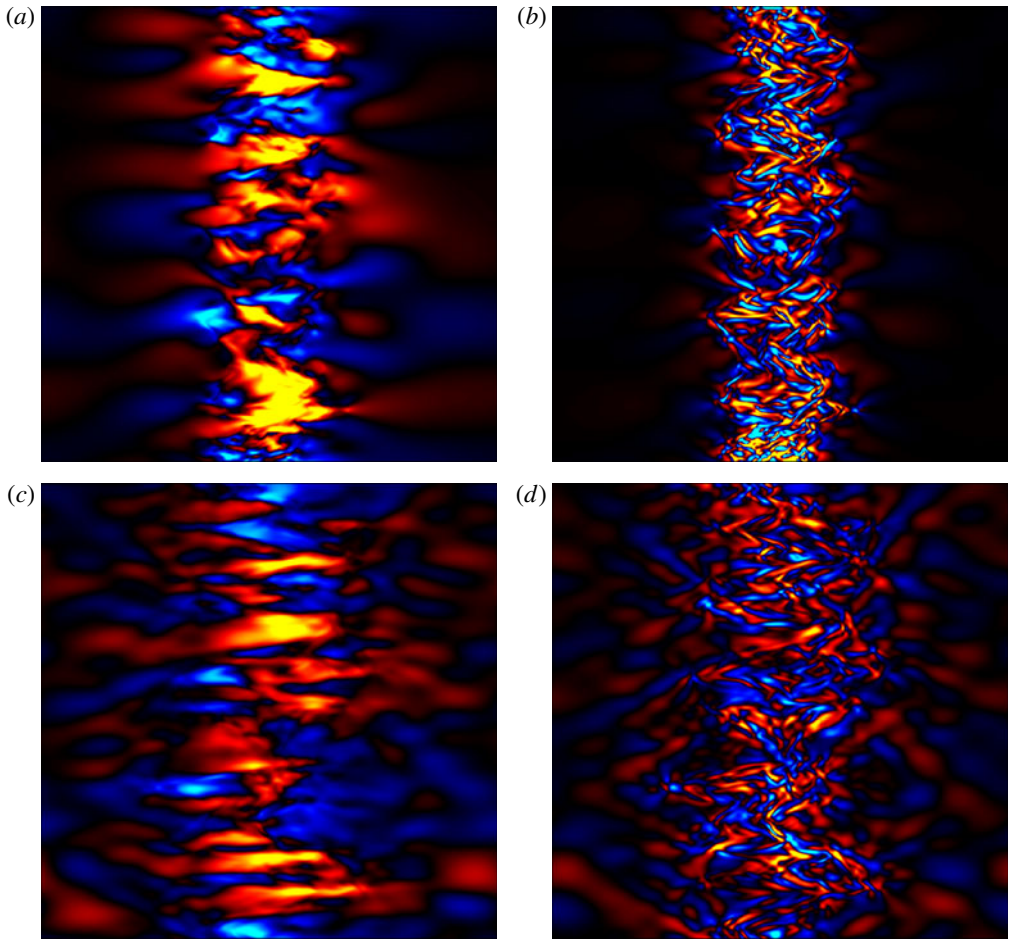


FIGURE 12. (Colour online) Vertical slices of u_x field in (*a,c*) and $\partial u_z/\partial z$ field in (*b,d*) at two different times (the slice is at $y = 0.1l_{box}$). Case F0.1 at times: (*a,b*) $Nt = 10.9$, (*c,d*) $Nt = 32.2$.

inclination of the diagonal waves is $\Theta = 50$–55° from the vertical, corresponding to a wave frequency $\omega = N\cos\Theta = 0.57N$–$0.64N$. The u_x field at the sides of the turbulent cloud is now a complicated superposition of horizontal and diagonal wave beams, since the waves with $\omega > 0$ also have an associated u_x field. It is evident from figure 12(*c*) that also the cloud interior has become layered in u_x, though through very different (nonlinear) dynamics compared to the largely linear dynamics on the sides of the turbulent cloud.

We have found evidence for the presence of two frequency bands for the internal gravity wave radiation from the turbulent cloud: horizontal internal gravity waves with $\omega \approx 0$ and inclined waves of finite frequency $\omega \approx 0.6N$. The second type of IGW is consistent with waves emitted from a well-mixed turbulent patch (Dohan & Sutherland 2003; Taylor & Sarkar 2007) and with IGWs emitted from a stratified turbulent wake (see Bonneton *et al.* 1993), but towards the lower end of the spectrum observed in a recent numerical study of wave radiation from a stratified turbulent wake at high *Re* (see Abdilghanie & Diamessis 2013). The horizontal waves are consistent

https://doi.org/10.1017/jfm.2013.612 Published online by Cambridge University Press

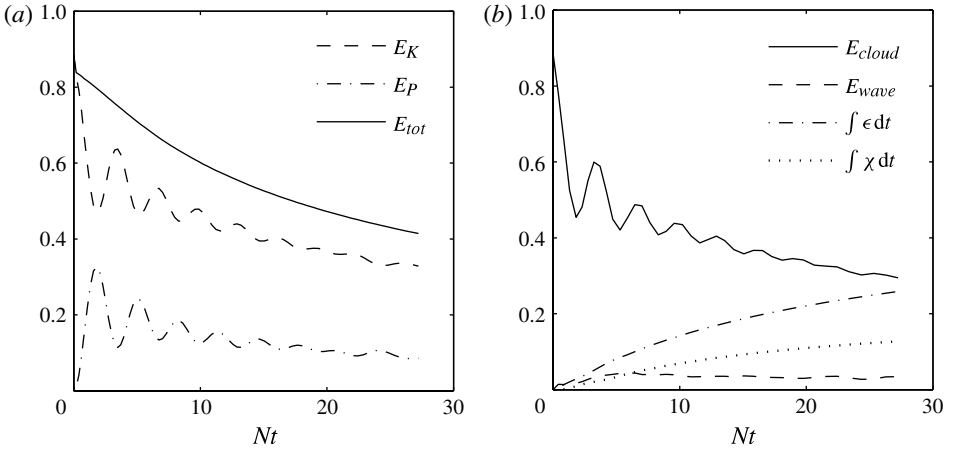


FIGURE 13. (*a*) Plots of the evolution with time of E_K, E_P and E_{tot} for simulation F0.1 (all energies are found by averaging their value throughout the entire box). (*b*) Evolution of energetics-related quantities for case F0.1: kinetic energy in the turbulent cloud $E_{cloud} = E_K - E_{wave}$, kinetic energy in propagating waves E_{wave} (found by integrating ahead of PV structures), and cumulative kinetic and potential energy dissipation.

with columnar modes emitted in front of intrusions (see Manins 1976; Maurer 2011). Apart from the continuously displaced dye lines, which are a signature of columnar wave activity, observed by Browand *et al.* (1987) and De Silva & Fernando (1998), these horizontal waves have not previously been observed or characterized in stratified turbulent cloud experiments or simulations. In part, this is because many previous studies (Linden 1975; Dohan & Sutherland 2003; Taylor & Sarkar 2007) considered turbulent patches that extended to cover the entire horizontal extent of the experimental/numerical domain, which directly rules out horizontal wave propagation. Horizontally localized turbulent clouds have been considered before by Basak & Sarkar (2006), but their use of $\partial u_z/\partial z$ as a signature of internal gravity waves means that they only observed inclined waves in their simulations. In figure 18 of their paper, vertical slices of ρ', ω_y and ω_x show the growth of layered structures out of the turbulent cloud; the authors interpret these structures as being solely due to intrusions, but they could represent both intrusions and horizontal waves travelling in front of them. It is interesting to note that in the same figure the authors show ω_z (a first-order approximation to the potential vorticity) and this quantity remains confined to the turbulent cloud, hinting at the fact that the horizontal structures to the sides of the cloud could in fact be internal gravity waves. The absence of a clear collapse event and of ensuing intrusions in stratified turbulent wakes (Lin *et al.* 1993; Abdilghanie & Diamessis 2013) could be the reason why horizontal IGWs have not been observed before in this context.

3.6. *Wave energetics*

The simulations were performed in the absence of forcing and the energy in the domain should therefore decay in time. A look at the kinetic energy in the box as a function of time shows that E_K does not decrease monotonically with time but rather presents large-amplitude oscillations (see figure 13*a*). These oscillations are in anti-phase with the oscillations on the potential energy plot (the potential energy

https://doi.org/10.1017/jfm.2013.612 Published online by Cambridge University Press

per unit mass at a point is $E_P = b^2/2N^2$), which suggests a process of exchange of kinetic and potential energy and hence the presence of gravity waves in the system. This is confirmed by the evolution of the total energy in the box, $E_{tot} = E_K + E_P$, which presents a classical viscous (and diffusive) decay. The period of the large-amplitude oscillations in figure 13(*a*) is $T \approx 0.07$ giving a frequency $\omega \approx 89.8 \approx 2N$, which is higher than the upper bound on the frequency of internal gravity waves in the system $\omega = N$. This apparent contradiction is due to the fact that if we are in the presence of IGWs, $u_x, u_y, u_z \propto \exp(\mathrm{i}\omega t)$ and the kinetic energy will be $E_K = (1/2)(u_x^2 + u_y^2 + u_z^2) \propto \exp(2\mathrm{i}\omega t)$, and so we can interpret the oscillations as being IGWs with $\omega = N$. It therefore appears that high-frequency waves are persistent in our runs and influence the total kinetic energy evolution. They are so visible on the plot of E_K because these waves are all created at $t = 0$ (and hence are in phase and will interfere constructively) as the density field $\rho'(t = 0) = 0$ adjusts to the turbulent velocity field imposed on it. After reaching their maximum amplitude these high-frequency waves gradually dissipate through the action of viscosity. Internal gravity waves with $\omega = N$ have zero group speed and correspond to trapped modes that remain confined to the initial turbulent cloud; they should be distinguished from the propagating internal waves with non-zero group speed that were identified in § 3.5.

To find the amount of kinetic energy in the propagating waves we integrated the kinetic energy in the regions ahead of the turbulent cloud as identified by the potential vorticity field. A threshold was set on $|\Pi|$ (typically taken as 0.1 % of $|\Pi|_{max}$) below which only propagating waves were assumed to exist. The result of this integration is given in figure 13(*b*) for run F0.1. It is clear that the kinetic energy in the propagating waves is a small but appreciable fraction of the kinetic energy left behind in the cloud $E_{cloud} = E_K - E_{wave}$, the maximum value of E_{wave}/E_{cloud} being $\approx 0.12 = 12\,\%$ for run F0.1. The evolution of E_{cloud}, similarly to the total kinetic energy in the box, presents oscillations created by internal waves with $\omega = N$, confirming that there are trapped modes that remain localized within the cloud. The radiated kinetic energy as a function of time does not present any visible oscillations and, after an initial transient, reaches an approximately steady value at $t = t_{peak}$. This suggests that the horizontal internal waves with $\omega \approx 0$ contain most of the radiated energy, while the off-axis waves do not contribute appreciably to the energetics. Such a view is consistent with the visualizations in figure 6 and with the experimental observations of figure 4, as in both cases only horizontal structures are observed.

In figure 13(*b*), the cumulative kinetic energy dissipation $\int_0^t \epsilon \, \mathrm{d}t$ and cumulative potential energy dissipation $\int_0^t \chi \, \mathrm{d}t$ are given, where $\epsilon = 2\nu S_{ij} S_{ij}$ is the kinetic energy dissipation rate and $\chi = (\mathscr{D}/N^2)\nabla b \cdot \nabla b$ is the rate of diapycnal mixing, and both quantities are volume averaged. Both ϵ and χ are confined to the turbulent cloud, as is confirmed by plots of these quantities averaged over vertical y–z planes as a function of x (not shown). By equipartition the kinetic energy of the propagating waves should equal their potential energy, which allows a direct comparison of E_{wave} to be made not only with $\int_0^t \epsilon \, \mathrm{d}t$ but also with $\int_0^t \chi \, \mathrm{d}t$. Hence, if we compare the kinetic energy in the propagating waves with the cumulative kinetic and potential energy dissipation we see that at $Nt = Nt_{peak} = 5.3$, E_{wave} is $\sim 50\,\%$ of the cumulative dissipation and 118 % of the cumulative mixing occurring within the cloud, and at the end of the run these values have dropped to 13 % and 27 % of the integrated dissipation and mixing respectively. These plots show that internal gravity wave radiation is an efficient source of energy dispersion from a cloud of turbulence, especially at the beginning of its evolution.

https://doi.org/10.1017/jfm.2013.612 Published online by Cambridge University Press

Simulation	Fr_0	Nt_{peak}	E_{wave}/E_{cloud} at $t = t_{peak}$(%)	$(E_{wave}/E_{cloud})_{max}$(%)
F0.2	0.2	4.8	10.6	10.9
F0.1	0.1	5.3	10.2	11.6
F0.03	0.032	6.5	10.1	16.2

TABLE 3. Energetics-related quantities for the propagating waves.

The percentage of kinetic energy held in the propagating waves relative to the kinetic energy in the cloud is given in table 3 at $t = t_{peak}$. Also the maximum value of E_{wave}/E_{cloud} is given for each decaying run. The fraction of radiated kinetic energy appears to be constant throughout the runs at $t = t_{peak}$ but the maximum value of this quantity is an inverse function of the Froude number, with the lowest-Fr case presenting the greatest wave energy percentage, equal to $\sim$16 %. This is a significant portion of the total E_K and means that propagating internal waves generated by a localized turbulence event could be important in the context of meteorology and oceanography as they could alter momentum and energy budgets in different regions of the atmosphere or oceans.

4. Discussion

4.1. *Stratified versus rotating turbulence*

It is of interest to revisit the analogy between stratified and rotating turbulent flows in the light of the results presented in the previous sections. Davidson *et al.* (2006) considered the linear initial-value problem of an eddy sitting in a rotating system and found that the component of angular momentum in the rotating reference frame along the direction of the rotation axis remains confined to the cylinder parallel to the rotation axis and circumscribing the eddy. The authors use this result to show that isolated eddies in a rotating fluid will deform as a result of linear internal wave propagation that preferentially channels energy along the rotation axis, giving rise to columnar structures. Experimental results are also presented showing that columnar wave-packets obeying linear theory emerge from a rotating turbulent cloud, thus corroborating the theory. In essence, in the rotating turbulent cloud problem, free and spontaneous emission of inertial waves from the cloud results in the formation of columnar structures. At first sight the analogy between rotating and stratified flows appears to carry through to the stratified turbulent cloud problem, where we have shown that quasi-linear internal waves form horizontal pancake-like structures. However, as evidenced by the experimental fluorescein visualizations, nonlinear fluid advection also results in the emergence of horizontal layered structures or intrusions from the turbulent cloud. The intrusion height roughly scales with the vertical wavelength obtained from the pearlessence visualizations. It is therefore likely that, as put forward by Browand *et al.* (1987), the intrusions push on the fluid immediately ahead of them and thereby create a steadily moving front that propagates into the quiescent region. This means that in the stratified turbulent cloud problem, forced emission of internal gravity waves (with the forcing provided by the intrusion motion) results in the creation of pancake structures. The analogy, which in any case was not a formal one, therefore seems to break down: the rotating case is a free emission problem, while the stratified case is a forced problem.

https://doi.org/10.1017/jfm.2013.612 Published online by Cambridge University Press

4.2. *Intrusions in experiments and simulations*

Moving now to a comparison between the experimental and numerical results, when inspecting the potential vorticity iso-surfaces in figure 7(*a*) one can notice that the structures are not very pronounced and the Π field remains localized even at late times. Recall that we use potential vorticity as a tracer in the same way as we used fluorescein as a tracer in the experiments; therefore the numerical intrusions shown by Π are far less pronounced than the experimental intrusions, to the point that one has doubts whether materially driven intrusions are present at all in the numerical results. To clarify this it is important to note that at high Reynolds numbers the relevant time scale for the potential vorticity is the advection time scale, or eddy turnover time, $T = l/u$ (see Riley & Lelong 2000). Now because the initial Froude number is low in all the runs considered thus far, the typical initial advection velocity u_0 will be much lower than the group speed of horizontal waves $c_g \sim Nl_0$, meaning that internal gravity waves will evolve much faster than the potential vorticity field. This explains why in figure 7 the waves have reached the cube boundaries, while the Π field is still very localized. If we express the time of figure 7 in eddy turnover times it corresponds to $t = 2T_0$, whereas the first experimental snapshot of figure 4 is at $t/T_0 = 9$ and the intrusions are really visible only beyond this time. Therefore we ran the simulation with $Fr_0 = 0.2$ again up to 18 eddy turnover times to check for the presence of intrusions in the simulation. In figure 14 vertical slices of the potential vorticity are presented at two y-locations, for run F0.2ext and for the high-Froude-number run F1.5, after the same number of eddy turnover times. Isolated intrusions have emerged from the turbulent cloud in both cases; the intrusions are less ordered than in the experiments, possibly due to the finite width of the turbulent slice, which is significantly deformed at this late time. In both runs with different Fr_0 the intrusions are about to reach the domain boundaries at the time $t \approx 16.5T_0$, which confirms that the eddy turnover time is indeed the correct time scale to describe the motion of the intrusions. The height of the intrusions seems to differ slightly across the two runs, with the F1.5 intrusions, for which the initial Froude number is higher, having a greater height than the F0.2 intrusions.

A similar variation in the intrusion height was observed in the experiments, with growing intrusion heights with increasing Froude number. To quantify this we measured a vertically averaged intrusion height from the fluorescein images (we did not attempt to do so in the simulations because of the lack of order of the numerical intrusions). A plot of the intrusion height h normalized by the initial turbulence length scale l_0 (estimated as the bar size b) as a function of the initial turbulent Froude number $Fr_0 = u_0/Nl_0$ is presented in figure 15. The line in figure 15 is a power law with the functional form $h/l_0 = 6.1(Fr_0)^{0.313}$, which provides a plausible fit to the data even though the experimental error bars are large. We now try to rationalize this behaviour of the intrusion height. The main physical ingredient of the analysis is that intrusions form as a result of the collapse of mixed pockets of fluid within the turbulent cloud. In this discussion we refer to collapse as the re-stratification of the density field that occurs in mixed fluid regions with $\rho_{tot} \approx$ const, with the associated horizontal spreading of fluid in the form of intrusions. We identify the onset of collapse as the moment when inertial forces that mix the density field approximately equal the buoyancy forces, i.e. when $Fr \sim 1$. Now, because $Fr_0 \gtrsim 1$ in all our experiments, the turbulence has time to mix the density field and consequently pockets of mixed fluid will grow. This process lasts until the Froude number has decayed to a value of order unity, when collapse occurs. Hence the height of the intrusions will depend on Fr_0, with greater Froude numbers allowing more time for the turbulence to mix the density field until it feels the effect of the stratification. To

https://doi.org/10.1017/jfm.2013.612 Published online by Cambridge University Press

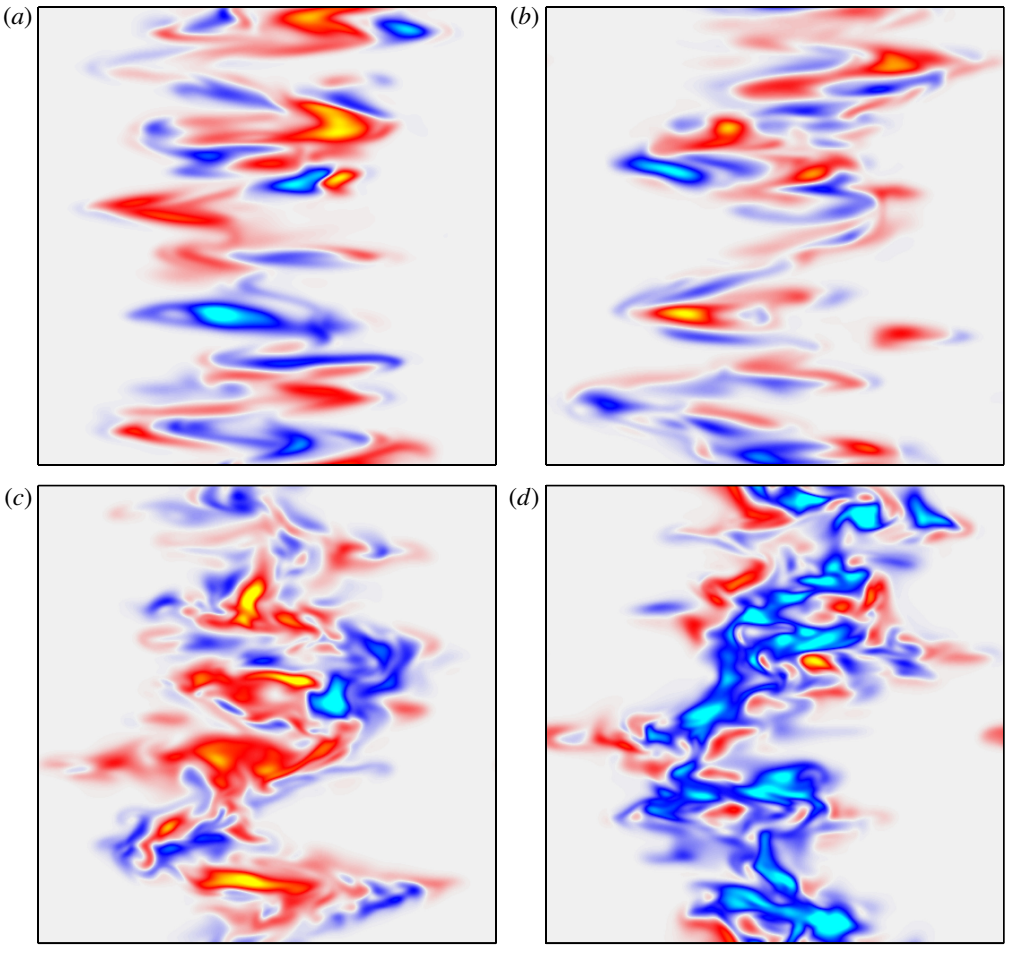


FIGURE 14. (Colour online) Vertical slices of Π field for (*a,b*) run F0.2ext at $t/T_0 = 16.5$ and (*c,d*) run F1.5 at $t/T_0 = 16.6$. Slices are x–z planes taken at (*a*) $y = 0.1l_{box}$, (*b*) $y = 0.9l_{box}$ for case F0.2ext and (*c*) $y = 0.1l_{box}$, (*d*) $y = 0.4l_{box}$ for case F1.5.

make any progress we need to estimate the initial evolution of the turbulent velocity and length scale to be able to estimate the time at which the turbulent Froude number becomes of order of unity. Because $Fr_0 \gtrsim 1$ in all the runs there will be a period of quasi-three-dimensional evolution and we might therefore use the estimates for energy decay in homogeneous isotropic turbulence, neglecting as a first approximation the inhomogeneity of the turbulent cloud. In a recent review Davidson (2011) starts from the well-established expression $\mathrm{d}u^2/\mathrm{d}t = -Au^3/l$ and finds the evolution of the kinetic energy and the integral length scale in decaying homogeneous isotropic turbulence. The evolution of u^2 and l can be written as

$$\frac{u^2}{u_0^2} = \left(1 + \frac{A}{n}\frac{u_0 t}{l_0}\right)^{-n}, \tag{4.1}$$

$$\frac{l}{l_0} = \left(1 + \frac{A}{n}\frac{u_0 t}{l_0}\right)^{1-n/2}, \tag{4.2}$$

https://doi.org/10.1017/jfm.2013.612 Published online by Cambridge University Press

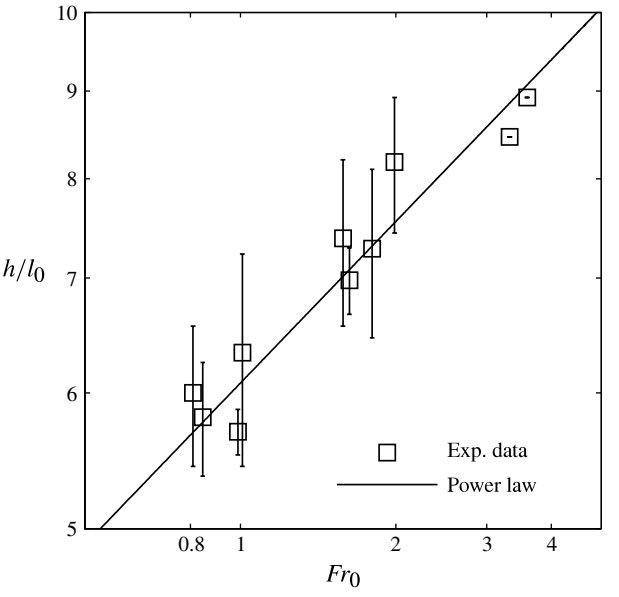


FIGURE 15. Intrusion height h normalized by initial integral length scale l_0 as a function of initial Froude number $Fr_0 = u_0/Nl_0$.

where u_0 and l_0 are the velocity scale and integral length scale of the turbulence at an initial time, taken as $t = 0$. Combining these two expressions a well-known result is obtained, notably that the integral time scale T of the turbulence grows linearly in time:

$$\frac{T}{T_0} = \frac{l/l_0}{u/u_0} = \left(1 + \frac{A}{n}\frac{u_0 t}{l_0}\right), \tag{4.3}$$

where T_0 is the initial integral time scale. Crucially this expression is also equal to the ratio between the initial Froude number Fr_0 and the Froude number at time t, that is $T/T_0 = Fr_0/Fr = [1 + (A/n)(u_0 t/l_0)]$. When $Fr = 1$, (4.3) gives $Fr_0 = [1 + (A/n)(u_0 t/l_0)]$, which is the quantity of which the power is taken in (4.2). Therefore it is also true that at collapse

$$\frac{l}{l_0} = (Fr_0)^{1-n/2}. \tag{4.4}$$

Up to this moment three-dimensional mixing takes place within the cloud, thus the vertical scale of the mixed fluid regions will be set by l. We have said that intrusions originate from such mixed regions, and hence it follows that the ensuing intrusion height is $h \sim l$. A corollary of this argument is that $h \sim l_b = u/N$ (where l_b is the buoyancy scale) or, equivalently, $h \sim l_{oz}$ (where $l_{oz} = (\epsilon/N^3)^{1/2}$ is the Ozmidov length scale). This follows from the fact that $l_{oz} = (\epsilon/N^3)^{1/2} \sim (u^3/lN^3)^{1/2} = Fr^{1/2} l_b \sim l_b$, when $Fr \sim 1$, where we have used the estimate $\epsilon \sim u^3/l$ and the fact that the turbulence is initially isotropic. Therefore (4.4) becomes

$$\frac{h}{l_0} \sim (Fr_0)^m, \tag{4.5}$$

https://doi.org/10.1017/jfm.2013.612 Published online by Cambridge University Press

which is an expression for the intrusion height (the substitution $m = 1 - n/2$ has been performed). Davidson (2011) reports a range of decay exponents, $n = 1.10$–1.37. The corresponding range for the exponent m in (4.5) is $m = 0.315$–0.45. The exponent obtained from the experimental data is $m = 0.313$, which is at the boundary of the range predicted by this semi-empirical model. The positive match with the experimental trend suggests that our physical picture is plausible, and that turbulent mixing inside the cloud causes the formation of the laterally spreading intrusions. In a different context, Spedding (2002) predicts the vertical scale of a stratified turbulent wake to be $L_v \sim Fr_0^{1/3}$, i.e. a power law with a very similar exponent to the one we obtained. The main assumption is that the vertical scale is set by the Ozmidov length scale at collapse, which as seen above is equivalent to assuming $Fr \sim 1$ as we have done.

5. Conclusions

The evolution of an inhomogeneous cloud of stratified turbulence, and the surrounding flow, is dominated by the growth of pancake structures, and these are composed of intrusions and horizontally propagating internal gravity waves that are forced by the intrusion motion. The series of events leading to layering in this problem is thought to be as follows: (*a*) mixing within the turbulent cloud creates regions of $\rho \approx$ const; (*b*) when these mixed regions reach a critical vertical scale $l \sim u/N$, they collapse under the action of gravity forming intrusions spreading to the sides of the cloud; (*c*) horizontal waves are forced by the intrusions and propagate at their level, enlarging the layer (as in figure 4). Such a layering mechanism is quite distinct from the previously proposed layering mechanisms of stratified turbulence, notably the decorrelation mechanism (see Lilly 1983) and the zig-zag instability (see Billant & Chomaz 2000). These mechanisms mainly affect the PV component of the flow, whereas the mechanism proposed here involves both potential vorticity motions and internal gravity waves. Because mixing within homogeneous stratified turbulence is not uniform but rather occurs in intermittent patches, this layering mechanism need not be restricted to the inhomogeneous problem under study and could be at work in a larger class of stratified turbulent flows.

Acknowledgements

The authors would like to thank Professor P. K. Yeung of Georgia Tech who provided the pseudo-spectral code used for the computations. A.M. gratefully acknowledges financial support received from EPSRC.

REFERENCES

ABDILGHANIE, A. M. & DIAMESSIS, P. J. 2013 The internal gravity wave field emitted by a stably stratified turbulent wake. *J. Fluid Mech.* **720**, 104–139.

ARMI, L. 1978 Some evidence for boundary mixing in the deep ocean. *J. Geophys. Res.* **83** (C4), 1971–1979.

BASAK, S. & SARKAR, S. 2006 Dynamics of a stratified shear layer with horizontal shear. *J. Fluid Mech.* **568**, 19–54.

BILLANT, P. & CHOMAZ, J.-M. 2000 Experimental evidence for a new instability of a vertical columnar vortex pair in a strongly stratified fluid. *J. Fluid Mech.* **418**, 167–188.

BILLANT, P. & CHOMAZ, J.-M. 2001 Self-similarity of strongly stratified inviscid flows. *Phys. Fluids* **13** (6), 1645–1651.

https://doi.org/10.1017/jfm.2013.612 Published online by Cambridge University Press

BONNETON, P., CHOMAZ, J.-M. & HOPFINGER, E. J. 1993 Internal waves produced by the turbulent wake of a sphere moving horizontally in a stratified fluid. *J. Fluid Mech.* **254**, 23–40.

BRETHOUWER, G., BILLANT, P., LINDBORG, E. & CHOMAZ, J.-M. 2007 Scaling analysis and simulation of strongly stratified turbulent flows. *J. Fluid Mech.* **585**, 343–368.

BROWAND, F. K., GUYOMAR, D. & YOON, S.-C. 1987 The behaviour of a turbulent front in a stratified fluid: experiments with an oscillating grid. *J. Geophys. Res.* **92** (C5), 5329–5341.

CALDWELL, D. R., BRUBAKER, J. B. & NEAL, V. T. 1978 Thermal microstructure on a lake slope. *Limnol. Oceanogr.* **23**, 372–374.

DALZIEL, S. B. 1992 Decay of rotating turbulence: some particle tracking experiments. *Appl. Sci. Res.* **49**, 217–244.

DAVIDSON, P. A. 2004 *Turbulence. An Introduction For Scientists and Engineers*. Oxford University Press.

DAVIDSON, P. A. 2011 The minimum energy decay in quasi-isotropic grid turbulence. *Phys. Fluids* **23** (8), 085108.

DAVIDSON, P. A., STAPLEHURST, P. J. & DALZIEL, 2006 On the evolution of eddies in a rapidly rotating system. *J. Fluid Mech.* **557**, 135–144.

DE SILVA, I. P. D. & FERNANDO, H. J. S. 1998 Experiments on collapsing turbulent regions in stratified fluids. *J. Fluid Mech.* **358**, 29–60.

DIAMESSIS, P. J., DOMARADZKI, J. A. & HESTHAVEN, J. S. 2005 A spectral multidomain penalty method model for the simulation of high Reynolds number localized incompressible stratified turbulence. *J. Comput. Phys.* **202** (1), 298–322.

DOHAN, K. & SUTHERLAND, B. R. 2003 Internal waves generated from a turbulent mixed region. *Phys. Fluids* **15** (2), 488–498.

FINCHAM, A. M., MAXWORTHY, T & SPEDDING, G. R. 1996 Energy dissipation and vortex structure in freely decaying stratified grid turbulence. *Dyn. Atmos. Oceans* **23**, 155–169.

FORTUIN, J. M. H. 1960 Theory and application of two supplementary methods of constructing density gradient columns. *J. Polym. Sci.* **44** (144), 505–515.

GILREATH, H. E. & BRANDT, A. 1985 Experiments on the generation of internal waves in a stratified fluid. *AIAA J.* **23** (5), 693–700.

GRANT, H. L., MOILLIET, A. & VOGEL, W. M. 1968 Some observations of the occurrence of turbulence in and above the thermocline. *J. Fluid Mech.* **34** (3), 443–448.

GREGG, M. C. 1987 Diapycnal mixing in the thermocline: a review. *J. Geophys. Res.* **92** (C5), 5249–5286.

HOGG, C. A. R., MARTI, C. L., HUPPERT, H. E. & IMBERGER, J. 2013 Mixing of an interflow into the ambient water of Lake Iseo. *Limnol. Oceanogr.* **58** (2), 579–592.

IVEY, G. N & CORCOS, G. M. 1982 Boundary mixing in a stratified fluid. *J. Fluid Mech.* **121**, 1–26.

KIMURA, Y. & HERRING, J. R. 1996 Diffusion in stably stratified turbulence. *J. Fluid Mech.* **328**, 253–269.

KUNDU, P. K. & COHEN, I. M. 2004 *Fluid Mechanics*, 3rd edn. Elsevier.

LIGHTHILL, J. 1978 *Waves in Fluids*. Cambridge University Press.

LILLY, D. K. 1983 Stratified turbulence and the mesoscale variability of the atmosphere. *J. Atmos. Sci.* **40**, 749–761.

LIN, J. T. & PAO, Y. H. 1979 Wakes in stratified fluids. *Annu. Rev. Fluid Mech.* **11**, 317–338.

LIN, Q., BOYER, D. L. & FERNANDO, H. J. S. 1993 Internal waves generated by the turbulent wake of a sphere. *Exp. Fluids* **15**, 147–154.

LINDBORG, E. 2006 The energy cascade in a strongly stratified fluid. *J. Fluid Mech.* **550**, 207–242.

LINDEN, P. F. 1975 The deepening of a mixed layer in a stratified fluid. *J. Fluid Mech.* **71**, 385–405.

LIU, Y. N., MAXWORTHY, T. & SPEDDING, G. R. 1987 Collapse of a turbulent front in a stratified fluid. 1 Nominally two-dimensional evolution in a narrow tank. *J. Geophys. Res.* **92** (C5), 5427–5433.

MAHRT, L. 1989 Intermittency of atmospheric turbulence. *J. Atmos. Sci.* **46**, 79–95.

https://doi.org/10.1017/jfm.2013.612 Published online by Cambridge University Press

MANINS, P. C. 1976 Intrusion into a stratified fluid. *J. Fluid Mech.* **74** (3), 547–560.

MAURER, B. D. 2011 Gravity-driven intrusions in stratified fluids. PhD thesis, University of California, San Diego.

POPE, S. B. 2000 *Turbulent Flows*. Cambridge University Press.

PRAUD, O., FINCHAM, A. M. & SOMMERIA, J. 2005 Decaying grid turbulence in a strongly stratified fluid. *J. Fluid Mech.* **522**, 1–33.

RILEY, J. J. & DE BRUYN KOPS, S. M. 2003 Dynamics of turbulence strongly influenced by buoyancy. *Phys. Fluids* **15** (7), 2047–2059.

RILEY, J. J. & LELONG, M.-P. 2000 Fluid motions in the presence of strong stable stratification. *Annu. Rev Fluid Mech.* **32**, 613–657.

SAVAŞ, Ö 1985 On flow visualization using reflective flakes. *J. Fluid Mech.* **152**, 235–248.

SPEDDING, G. R. 2002 Vertical structure in stratified wakes with high initial Froude number. *J. Fluid Mech.* **454**, 71–112.

SPEDDING, G. R., BROWAND, F. K. & FINCHAM, A. M. 1996 Turbulence, similarity scaling and vortex geometry in the wake of a towed sphere in a stably stratified fluid. *J. Fluid Mech.* **314**, 53–103.

STAPLEHURST, P. J. 2007 Structure formation in rotating turbulence. PhD thesis, University of Cambridge.

TAYLOR, J. R. & SARKAR, S. 2007 Internal gravity waves generated by a turbulent bottom Ekman layer. *J. Fluid Mech.* **590**, 331–354.

THORPE, S. A. 1982 On the layers produced by rapidly oscillating a vertical grid in a uniformly stratified fluid. *J. Fluid Mech.* **124**, 391–409.

WAITE, M. L. & BARTELLO, P. 2004 Stratified turbulence dominated by vortical motion. *J. Fluid Mech.* **517**, 281–308.

YEUNG, P. K. 2001 Lagrangian characteristics of turbulence and scalar transport in direct numerical simulations. *J. Fluid Mech.* **427**, 241–274.

YEUNG, P. K. & POPE, S. B. 1989 Lagrangian statistics from direct numerical simulations of isotropic turbulence. *J. Fluid Mech.* **207**, 531–586.

https://doi.org/10.1017/jfm.2013.612 Published online by Cambridge University Press